Energy Levels of Atomic Aluminum with Hyperfine Structure

Edward S. Chang

Department of Physics and Astronomy, University of Massachusetts, Amherst, Massachusetts 01002

A new energy level table for Al I has been constructed to include hyperfine structure from observations within the last decade. Improvement in accuracy over older tables is about an order of magnitude. The analysis of high-l Rydberg levels utilizing the polarization formula results in a new value for the ionization potential which is $0.110 \, \text{cm}^{-1}$ or five standard deviations above the old value.

Key words: aluminum; atomic data; energy levels; hyperfine structure; spectra.

1. Introduction

The singly excited states of Al I can be described simply as those of a Rydberg electron with principal and orbital quantum numbers n and l orbiting around an ionic core with a $3s^2$ configuration outside of a Ne-like inner shell. In this picture the angular momentum of the core is due entirely to the nucleus, whose sole isotope has a spin $I = 5/2$. Its interaction with the electronic angular momentum gives rise to the hyperfine structure, which would fall off as the inverse third power of n and of l in the simple picture. However, in reality the low-lying $3s \, 3p^2$ configuration perturbs the $ns^2 S$ and the $nd \, ^2D$ series. Consequently, the lower members of both $3s^2 \, ns \, ^2S$ and $3s^2 \, nd \, ^2D$ series have hyperfine splittings comparable to those of the ground $3p \, ^2P$ state.

A comprehensive energy level table was given by Eriksson and Isberg[1] (referred as EI). Nearly complete hyperfine structures were tabulated for the lowest member of the ^2S, ^2P, and ^2D series. The table has been extended[2] to include higher ^2D (and ^2S) levels and doubly excited states, but to conform to format, the information on hyperfine structure was removed.

In the last decade, the hyperfine structure of many excited states have been measured with high-resolution lasers on atomic beams[3–5] and with level crossing techniques.[6] The measured splittings are often as large as $0.01 \, \text{cm}^{-1}$. Therefore, they must be properly accounted for in compiling energy levels when accuracy in the $0.001 \, \text{cm}^{-1}$ range is desired. So in Sec. II the experimental data on hyperfine structure (HFS) is reviewed. In cases where data are not available, schemes for interpolation or extrapolation are discussed.

Recently the infrared spectrum has been observed by Biemont and Brault[7] (referred as BB) from 1800 to 9000 cm^{-1} with an accuracy in the third decimal place. Hyperfine splittings were often partially resolved but not explicitly

identified. In order to facilitate identification, the line intensity formulas for the hyperfine components are developed in Sec. 3. With these in hand, the infrared lines of BB are utilized to work out the energy levels of Al I including hyperfine structures in Sec. 4. Usually the strongest line within a fine structure (FS) transition is used to fix the highest total angular momentum F sub-level. Then the rest of the hyperfine components can be determined from the more accurate laser data of Sec. II. Consistency tests from the weaker hyperfine transitions and from the Ritz combination principle suggest that the new energy levels are accurate to ~ 0.003 cm^{-1}.

In Sec. 5, some high-l Rydberg transitions are combined with the solar emission line data[8] to fit the polarization formula.[9,10] Together with the low-l energy levels in Sec. 4, I determine a new value for the ionization potential (IP). It turns out to be $0.11 \, \text{cm}^{-1}$ higher than the old value of EI, based on the $nf \, ^2F$ series. The discrepancy is explained and implications for applying the polarization formula to this series are discussed.

2. Hyperfine Structure

It has long been recognized that the hyperfine splittings in Al I are as large as several hundredths of a cm^{-1}. Therefore, they need to be properly accounted for in constructing accurate energy levels from spectral data. The standard formula is given by[11]

$$E_{hfs} = \frac{1}{2} AC + \frac{1}{2} B \times \left[\frac{3}{8} C(C+1) - \frac{1}{2} I(I+1)J(J+1) \right]. \quad (1)$$

For aluminum, the nuclear spin I has the sole value of 5/2, and C is defined by

$$C = F(F+1) - I(I+1) - J(J+1). \quad (2)$$

In Eq. (1), A in the first term is the magnetic dipole constant and B in the second is the electric quadrupole constant.

Measured values of A and B are presented in Table 1.

Table 1. Hyperfine constants for Al I.

$2S+1_{L_J}$	n	A(MHz)	B(MHz)
$^2S_{1/2}$	4	421(15)[a]	0
$^2P_{1/2}$	3	502(0)[b]	0
	5	20(2)[c]	0
$^2P_{3/2}$	3	94(0)	18.8(3)[b]
	6	5.7(0)	0.5(0)[d]
	7	3.3(0)	0.3(0)[d]
	8	2.1(0)	0.2(0)[d]
$^2D_{3/2}$	3	$-99(1)$	$-13(4)$[e]
	4	$-72(8)$[e]	$\cdots$
$^2D_{5/2}$	3	182(1)	22(12)[e]
	4	204(3)[e]	$\cdots$
	5	162(16)[f]	$\cdots$

[a] Ref. 3.
[b] EI, Ref. 1.
[c] Ref. 4.
[d] Ref. 5.
[e] Ref. 6.
[f] BB, see text in Sec. 4.

For spectroscopic terms with $J \leqslant 1/2$, B vanishes automatically. As for the other terms, B is either an order of magnitude less than A or undetermined. Therefore, I retain B only for the $n = 3$ levels, assuming its value to be negligibly small for all $n \geqslant 4$.

As is evident from Table 1, values of A have by no means been measured for all levels. The most complete set, the np $^2P_{3/2}$ series, is shown on a log–log plot against the effective quantum number[1] n^* in Fig. 1(a). The data fit a straight line reasonably well, yielding $A = 196$ MHz$/n^{*2.6}$. On the same plot are shown the only two measured values for the $^2D_{3/2}$ states. Their values are actually negative, implying an inverted hyperfine structure. A straight line extrapolation is assumed, but even then the large error bar on the $n = 4$ value renders the extrapolated values rather uncertain. Fortunately they are small; even the $5d$ $^2D_{3/2}$ hyperfine splitting is already < 0.01 cm^{-1}.

Figure 1(b) is a similar graph for the other cases where the values for A are approximately one order of magnitude larger. A straight line fit for the np $^2P_{1/2}$ series, yields $A = 2220$ MHz$/n^{*3.6}$. For the ns $^2S_{1/2}$ series, only the $n = 4$ value has been measured. However, it is known that the quantum defect is virtually constant and that the measured lifetimes[3] scale as n^{*3}. Hence it is surmised that this series is only weakly perturbed by the $3s3p\,mp$ ^2S series, so the A values should scale as the inverse of n^{*3}. Turning to the nd $^2D_{5/2}$ series, the two measured values for A actually increase with n^*! This bizarre behavior and indeed the negative A values for the $^2D_{3/2}$ series have been shown[12] as due to the strong perturbation of the $3s3p^2$ ^2D state. From the infrared measurements of BB which partially resolve some hyperfine structures, I infer in Sec. 4 an A value for the $5d$ $^2D_{3/2}$ level which is lower than that for the $4d$ $^2D_{3/2}$ level. In Table 2, the hyperfine splittings are calculated according to Eqs. (1) and (2) with the hyperfine constants in Table 1, with the inferred accuracy of 0.0001 cm^{-1} or better. I estimate that extrapolated values (in parentheses) to be accurate to at least 0.001 cm^{-1}.
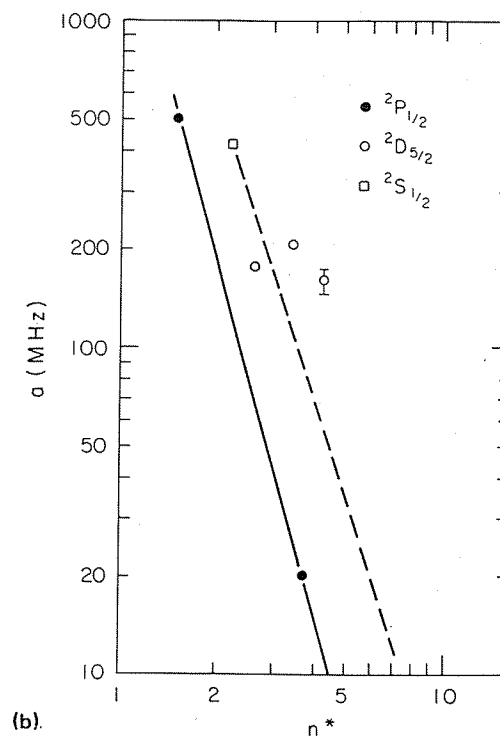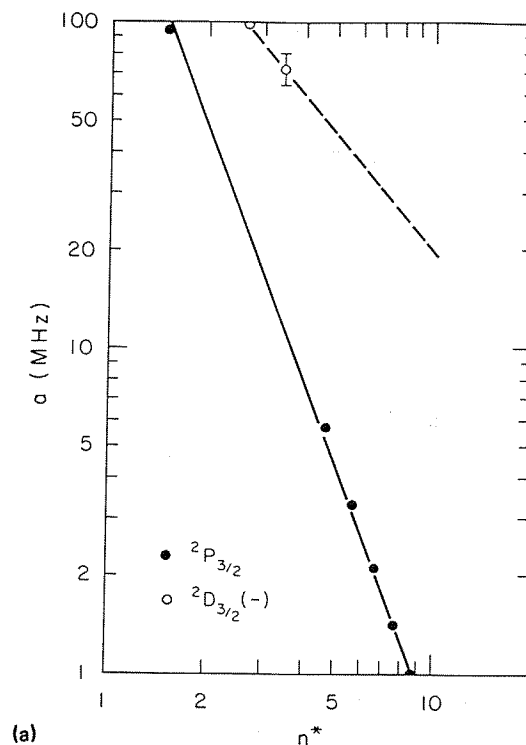

FIG. 1. (a) Experimental HFS magnetic dipole constants in MHz plotted against the effective quantum number for the $^2P_{3/2}$ and the $^2D_{3/2}$ series. (b) Same plot for the $^2S_{1/2}$, $^2P_{1/2}$, and the $^2D_{5/2}$ series.

Table 2. Hyperfine sub-levels in cm^{-1}.

n	$^2S_{1/2}$	$F=2$	3	$^2P_{1/2}$	$F=2$	3
3		$\cdots$	$\cdots$		-0.0293	0.0209
4		-0.0246	0.0176		(-0.0037	0.0027)
5		(-0.0077	0.0055)		-0.0012	0.0008
6		-0.0034	0.0024		(-0.0005	0.0004)
7		(-0.0018	0.0013)		(-0.0002	0.0002)
8		(-0.0011	0.0008)			

n	$^2P_{3/2}$	$F=1$	2	3	4
3		-0.0160	-0.0103	-0.0011	0.0119
4		(-0.0040	-0.0025	-0.0002	0.0028)
5		(-0.0017	-0.0011	-0.0001	0.0012)
6		-0.0010	-0.0006	-0.0000	0.0007
7		-0.0006	-0.0004	-0.0000	0.0004

	$^2D_{3/2}$	$F=1$	2	3	4
3		0.0178	0.0106	0.0004	-0.0125
4		0.0126	0.0078	0.0006	-0.0090
5		(0.0094	0.0058	0.0004	-0.0068)

	$^2D_{5/2}$	$F=0$	1	2	3	4	5
3		-0.0534	-0.0472	-0.0349	-0.0166	0.0077	0.0378
4		-0.0595	-0.0527	-0.0391	-0.0187	0.0085	0.0425
5		-0.0472	-0.0418	-0.0310	-0.0148	0.0065	0.0338

3. Line Intensities

Most of the present energy levels are derived from the Fourier transform spectroscopic data of BB, which provided identification with the fine structure quantum numbers J. In many instances several unidentified hyperfine components are given with their observed intensities. Assuming that the initial state is populated according to its statistical weight, the line intensity is proportional to[13]

$$I^{n'L'J'F'}_{nLJF} = (2J+1)(2J'+1)(2F+1)(2F'+1)$$

$$\times \begin{Bmatrix} 1 & J & J' \\ S & L' & L \end{Bmatrix}^2 \begin{Bmatrix} 1 & F & F' \\ I & J' & J \end{Bmatrix}^2, \quad (3)$$

where the curly bracket indicates a Wigner 6-j symbol. In Eq. (3), the unprimed and the primed quantum numbers are symmetrical, so one set belongs to the initial and the other set to the final state.

When the hyperfine splitting of one state is unresolved (the primed set), summation in F' yields

$$I^{n'L'J'}_{nLJF} = (2F+1)(2J'+1) \begin{Bmatrix} 1 & J & J' \\ 1/2 & L' & L \end{Bmatrix}^2, \quad (4)$$

where a doublet ($S = 1/2$) has been explicitly assumed. In some instances e.g., ^2D–^2F transitions, it is possible that even the FS of one state is unresolved while the HFS of the other is (partially) resolved. Then the sum rule again is applied to give the intensities

$$I^{n'L'}_{nLJF} = \frac{2F+1}{2L+1}. \quad (5)$$

For brevity, the indices n, L, n', and L' in Eqs. (3), (4), and (5) will often be deleted. Combining these results with the HFS splittings of Table 2 proves to be adequate to completely identify the infrared emission lines observed by BB.

4. Low L Levels

4.1. The ^2S–^2P Transitions

Starting with the already accurately measured ground $3p$ configuration as given by EI, I slightly revise the $4s$ hyperfine levels to reflect the spacings of Table 2, which utilizes the new value for A (Table 1). The BB data for the $4s$–$4p$ transition reveal two "doublets" whose splitting closely matches the $4s$ hyperfine splitting of 0.042 cm^{-1}. On the other hand, Table 2 reveals that the corresponding splittings in the ^2P levels are smaller by an order of magnitude. According to Eq. (4), the $4s$–$4p$ intensity ratios

$$I^{1/2}_{1/2\;3} : I^{1/2}_{1/2\;2} : I^{3/2}_{1/2\;2} : I^{3/2}_{1/2\;2}$$

are 7:5:14:10 which agree well with the observed intensities[7] of 50000, 36300, 100000, and 71000. In addition, the asterisks after the first and the third lines indicate that these measurements correspond to the most intense hyperfine components of the ^2P state. From Eq. (3), I find that they are $I^{1/2\;2}_{1/2\;3}$ and $I^{3/2\;4}_{1/2\;3}$, respectively. Thus, these $4p$ hyperfine levels are evaluated from the BB data and entered into Table 3. Obviously the remaining $4p$ hyperfine levels can now be accurately obtained from Table 2.

The transition $4p$–$5s$ reveals only two lines (without asterisks) implying that even the HFS splitting of the $5s$ level, 0.013 cm^{-1}, was not resolved. Nevertheless, I presume that the peak-finding computer programs employed in BB's data analysis would select out $I^{5s\;1/2\;3}_{4p\;1/2\;2}$ and $I^{5s\;1/2\;3}_{4p\;3/2\;4}$, respectively. Indeed upon addition of the transition wavenumbers to the respective $4p$ fine and hyperfine levels, I obtain two identical values for the position of the $5s\;F=3$ sub-level. Similarly, the higher members of the ns and np series are found in this manner. In several cases, a level can be deter-

EDWARD S. CHANG

Table 3. Al I energy levels.

	J	F			J	F	
4s	1/2	2	25 347.732	3d	3/2	4	32 435.458
	1/2	3	25 347.774		5/2	5	32 436.836
5s	1/2	3	37 689.412	4d	3/2	4	38 929.404
6s	1/2	3	42 144.413		5/2	5	38 934.011
7s	1/2	3	44 173.134	5d	3/2	4	42 233.735
8s	1/2	3	45 457.245		5/2	5	42 237.817
				6d	3/2	4	44 166.398
3p	1/2	2	− 0.029		5/2	5	44 168.847
	1/2	3	+ 0.021				
	3/2	1	112.045	4f	5/2		41 319.390
	3/2	2	112.051		7/2		41 319.398
	3/2	3	112.060	5f	5/2		43 831.101
	3/2	4	112.073		7/2		43 831.105
4p	1/2	2	32 949.803	6f	5/2		45 194.703
	3/2	4	32 965.642		7/2		45 194.705
5p	1/2	2	40 271.977				
	3/2	4	40 277.884	5g			43 875.752
6p	1/2	2	43 335.024	6g			45 221.721
	3/2	4	43 337.890	7g			46 033.274
7p	1/2	2	44 919.666				
	3/2	4	44 921.287	6h			45 227.555
				7h			46 037.096
				7i			[46 038.259]
				IP			48 278.480(3)

EI's center of gravity position, the $^2D_{3/2}$ sub-levels differ by more than 0.03 cm^{-1} from those given by EI.

Next the 4d sub-levels are mostly accurately determined from the strong 4p–4d array. Here four hyperfine components are seen in the fine structure transition $^2P_{3/2}$–$^2D_{5/2}$. Recalling that the HFS in the p level is very small, it is easy to understand that these lines correspond to different hyperfine levels of the $^2D_{5/2}$ level. According to Eq. (4), the intensity ratios in the order of decreasing values of F are 33:27:21:15:9:3. The observed ratios for the four (strongest) components are 13200:11500:10000:8900. Clearly the agreement worsens as F decreases. A likely explanation is that the undetermined constant B is actually quite significant for the 4d $^2D_{5/2}$. As shown by Eq. (1), the quadrupole HFS has a parabolic structure. Then the positions of the lower F components are shifted in the direction of the higher F components. From the experimental viewpoint, the effect is to shift the positions of the $F=0$ and 1 components into the vicinity of the $F=2$ and 3 components. Anyway, the four measured peaks at 5968 cm^{-1} with the decimal of 0.366, 0.335, 0.303, and 0.290 are assumed to be due to $I^{5/2}_{3/2}{}^5_4$, $I^{5/2}_{3/2}{}^4_3$, $I^{5/2}_{3/2}{}^3_2$, and $I^{5/2}_{3/2}{}^2_2$, respectively. (The value 0.335 differs from the BB value of 0.355 because it is derived from the HFS of Table 2, and has been found by BB to fit the observed profile better). Since the strongest peak is due to a unique HFS transition, I assume it locates the 4d $^2D_{5/2}$ ($F=5$) level unambiguously. Then the other sub-levels with $F=4$ decreasing to 0 can be calculated from Table 2. The calculated $^2D_{5/2}$ sublevels are compared with those inferred from the other three line centers, and found to have small discrepancies of 0.000, 0.004, and 0.001 cm^{-1}. For the remaining two lines in the same array, the measured intensities of 2300 and 11500 indicate that they correspond to $I^{4d\ 3/2}_{4p\ 3/2}{}^4$ and $I^{4d\ 3/2}_{4p\ 1/2}{}^4$ whose theoretical values are 4.5 and 22.5, respectively. Their inferred positions for the 4 $^2D_{3/2}$ ($F=4$) level agree perfectly and are entered into Table 3.

In principle, the 4d–6p array also measured by BB provides an independent check for the positions of the 4d sublevels. However, these lines are about four orders of magnitude weaker. Further, even the strongest lines here are blended. Nevertheless the discrepancies with levels from the 4p–4d array are only ~0.01 cm^{-1}.

Similarly the 5p–5d array can be utilized to determine the positions of the 5d levels. Experimentally found levels are compared with calculated ones when possible. The discrepancy is no larger than 0.002 cm^{-1}. Although the 5d levels can also be deduced from the 5d–7p array, the actual data only consist of two blended lines. Their resolutions are an order of magnitude lower, so they are not useful for the purpose of accurate energy determination.

Finally, the two faint lines in the 5p–6d array are used to calculate the positions of the 6d $^2D_{3/2}$ and $^2D_{5/2}$ levels. From the 6p levels in Table 3, one infers wavenumbers of 831.380 and 830.966 cm^{-1} for the 6p–6d $^2D_{1/2}$–$^2D_{3/2}$ and $^2P_{3/2}$–$^2D_{5/2}$ lines. The above provide even stronger confirmation of the identification[10] of the solar emission lines at 831.374 and 830.957 cm^{-1}. Since the solar lines are much stronger than the faint 5p–6d lines, they are utilized to fix the positions of the 6d levels in Table 3.

mined from more than one measurement. A consistency check reveals that the discrepancy seldom exceeds 0.003 cm^{-1}. In such cases, the intensity-weighted average is entered into Table 3.

4.2. The ^2P–^2D Transitions

The 3d levels in EI were inferred from the ultraviolet 3p–3d lines measured with diffraction gratings. In only one instance was the hyperfine structure resolved and then in just the $^2P_{1/2}$ but not in the $^2D_{3/2}$ state. Consequently, the level positions were uncertain by at least the ^2D hyperfine splittings which ranged over some 0.01 cm^{-1}. From the BB infrared data, the 3d levels can be evaluated from the 3d–5p transitions. Here only three weak lines have been observed, corresponding to the well-resolved fine structure. However, the observed intensity ratios of 17:13:8 deviate from the expected fine structure ratios of 5:9:1. Most likely the observed line intensities correspond to $(I^{5p\ 1/2}_{3d\ 3/2}{}_3 + I^{5p\ 1/2}_{3d\ 3/2}{}_4):I^{5p\ 3/2}_{3d\ 5/2}{}_5:I^{5p\ 3/2}_{3d\ 3/2}$ (all HFS), which yield the intensity ratios 20:16.5:6 according to Eq. (4). Note that the hyperfine splittings are much smaller in the p state than in the d state. From the first two lines and the known 5p levels, I obtain the positions of the sub-levels 3d $^2D_{3/2}$ ($F=4$) and $^2D_{5/2}$ ($F=5$), respectively. As a check, the position of the 3d $^2D_{3/2}$ ($F=4$) sub-level is found from the weakest line to be consistent to within 0.003 cm^{-1}. While the $^2D_{5/2}$ sub-levels agree reasonably well with

4.3. The ^2D–^2F Transitions

In the hydrogenic theory[14] the HFS of the n^2F levels are six times smaller than those of the np ^2P level. From the $4p$ splittings of ~ 0.005 cm^{-1} in Table 2, one expects the HFS of all ^2F levels to be < 0.001 cm^{-1}. Indeed even the fine structure for the $4f$ state is only 0.008 cm^{-1} in the hydrogenic theory,[14] as was apparently found to be the case experimentally for Al I by EI. Thus the FS in f levels cannot be resolved in the ^2D–^2F transitions of BB, whereas the HFS in the lower d levels is often resolved.

In the strong $4d$–$4f$ array, the first four lines have measured intensities of 4000, 3200, 2500, and 2000. They correspond well to the theoretical ratios from Eq. (5) of 11:9:7:5 for $F = 5, 4, 3$, and 2 in the $^2D_{5/2}$ state. It is interesting that in the strongest line, the asterisk here actually indicates the presence of the two FS (rather than the usual HFS) levels in the ^2F state. Thus, the strongest line would place the $4f$ $^2F_{7/2}$ level at 41 319.394 while the other lines give the decimal as 0.395, 0.396, and the blend of 0.402 and 0.390. In the same array, the remaining two lines are both observed to have intensities of 3200. One is undoubtedly the $F = 4$ component of the $^2D_{3/2}$–$^2F_{5/2}$ transition with a theoretical intensity of 9. Thus, the position of the $4f$ $^2F_{5/2}$ level is determined to be 41 319.390 cm^{-1}. The asterisk on the other line indicates that the $F = 3$ component is blended with the $F = 2$ one. The resulting level for $4f$ $^2F_{5/2}$ is several 0.001 cm^{-1} lower and less reliable. Accepting the firmer number, then the fine structure splitting places the $^2F_{7/2}$ level at 41 319.398, which is commensurate with the average of its earlier determinations. From the $3d$–$4f$ transitions, the $^2F_{5/2}$ and $^2F_{7/2}$ levels are found to be 0.003 and 0.004 cm^{-1} higher. Since these transitions are an order of magnitude weaker, I take these evaluations as confirmation of the above energy determinations. In comparison with those of EI, my ^2F levels are 0.018 cm^{-1} higher.

Turning to the very weak $4d$–$5f$ array, the three lines identified by BB as $^2D_{5/2}$–$^2F_{5/2}$ transitions actually belong to the $^2D_{5/2}$–$^2F_{7/2}$ transitions where intensities are 20 times larger. They correspond to the $F = 5, 4, 3$ (blended with 2) sub-levels of the D state. Thus, they place the $5d$ $^2F_{7/2}$ level at 43 831.102, 43 831.105, or 43 831.109 cm^{-1}. Their average value is 43 831.105 cm^{-1}, and the hydrogenic formula then fixes the $5f$ $^2F_{5/2}$ level at 0.004 cm^{-1} lower, which also agrees with EI's value for the $5f$ splitting. In the remaining line, $^2D_{3/2}$–$^2F_{5/2}$, the HFS was not resolved. If the line center were one third of the way between the $F = 3$ and $F = 4$ components, the $5f$ $^2F_{5/2}$ level would lie at the above position.

The $6f$ levels prove to be even more difficult to fix from the BB data. From the $4d$–$6f$ array, the $^2D_{5/2}$–$^2F_{7/2}$ lines with HFS partially resolved were measured only to two decimal places because of their broadened profiles. Specifically, these three lines place the $6f$ $^2F_{7/2}$ at 45 194.69 cm^{-1}. On the other hand, the $^2D_{3/2}$–$^2F_{5/2}$ line, with unresolved HFS, determines the $6f$ $^2F_{5/2}$ level at 45 194.691 cm^{-1} if the same assumption were made about the line center. Then the hydrogenic FS places the $6f$ $^2F_{7/2}$ at 0.002 cm^{-1} higher. Unfortunately, the two $5d$–$6f$ lines have been measured only to two decimal place accuracy. Their broadened profiles are due primarily to the HFS of the $5d$ states. As an unknown number of components are included in the profile, definitive energy levels cannot be extracted from the BB data. In Sec. 5, it will be shown that the $6f$ levels can be more accurately determined from a solar emission line.

5. High L Levels and the Ionization Potential

For the case of Mg I, it has been demonstrated that Rydberg levels with $l \geqslant 4$ are accurately given by

$$E_{nl} = IP - R/n^2 - \Delta_r - \Delta_p. \tag{6}$$

In Eq. (6) IP is the ionization potential, the Rydberg constant R for Al is 109 735.086 cm^{-1}, and Δ_r is the small relativistic correction.[9,10] The polarization energy is

$$\Delta_p = A\,P(n,l)\,[1 + kq(n,l)], \tag{7}$$

where P and q are well-known functions, e.g., tabulated by Edlen.[9] The parameters A (the core polarizability, not to be confused with the magnetic dipole constant) and k are to be fitted from high l data. In Table 4, high-l transitions from the BB data and previously observed solar emission lines[8] appropriate for this fitting are tabulated. Best fit values are $A = 23.936$ and $k = -0.274$. The present value of A is more accurate than the earlier value[8] of 23.9, based solely on the solar lines and assuming a vanishing value for k. Calculated values for the transitions are shown in the last column. They are clearly in agreement with all data to within the 0.003 cm^{-1} uncertainty of the observed values.

The ionization potential may now be obtained in several independent ways. From the $4f$ $^2F_{7/2}$ level in Table 3, one may add the $4f$–$7g$ wavenumber and the $7g$ term value from the polarization formula to obtain 48 278.483(3). Alternatively one may add the $4f$–$6g$ and the $6g$–$7h$ wavenumbers and then the $7h$ term value to find 48 278.479(3). If instead one adds the $4f$–$5g$ and the $5g$–$7h$ wavenumbers, one gets 48 278.476(10). The uncertainties given are experimental and do not include errors in the polarization formula, Eqs. (6) and (7). Starting with the $5f$ $^2F_{7/2}$ level, one may add the $5f$–$7h$ wavenumber to obtain 48 278.464(10). In all, the statistical average value of the ionization potential is found to be 48 278.480(3) cm^{-1}. This value is 0.11 cm^{-1} higher than the EI value, far exceeding their estimated error of 0.02 cm^{-1}.

Combining with the solar emission line $6f$–$7g$ at 838.565 and the $7g$ term value, I find the $6f$ $^2F_{7/2}$ level to lie at 45 194.705 cm^{-1}. This value is preferred over those obtained from d–f transitions which centered around 45 194.69 cm^{-1} in Sec. 4. It is entered into Table 3 with the $6f$ $^2F_{5/2}$ level at the theoretical 0.002 cm^{-1} below it.

Table 4. High-l transitions and the polarization formula

Transition	σ_{ob} (cm^{-1})	σ_{calc} (cm^{-1})
$6h$–$7i$[a]	810.704(3)	810.706
$6g$–$7h$[a]	815.375(3)	815.376
$5g$–$6g$[b,c]	1345.969(1)	1345.967
$5g$–$7g$[b,c]	2157.522(1)	2157.519
$5g$–$7h$[b]	2161.340(10)	2161.343

[a] Solar emissions, Ref. 8.
[b] Lab. emission, Ref. 7.
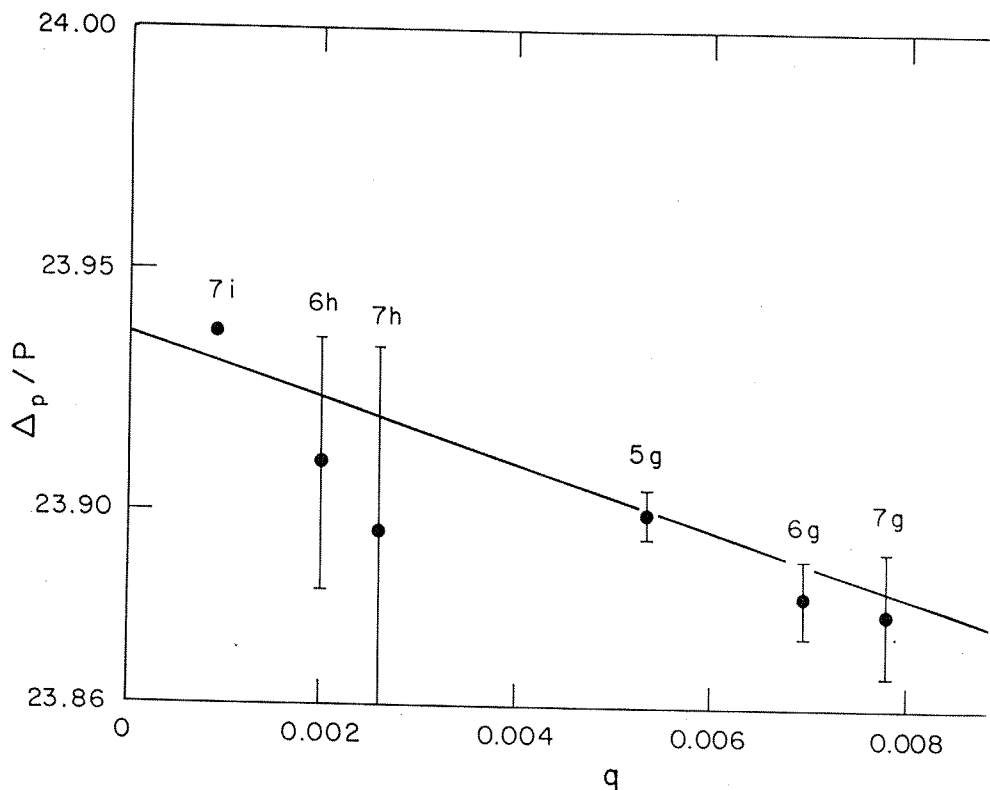[c] Combination involving the $4f$ level.

FIG. 2. Plot for polarization formula for the $l \geqslant 4$ levels in Al I. Note the expanded ordinate scale, where the the intercept yields a very accurate values for A.

The remainder of Table 3 is easily filled as follows. The g levels are found from the $4f$–ng transitions of BB. From the $6g$ level, the $7h$ level is determined from the solar emission line.[8] Similarly, another solar line locates the $6h$ from the $7i$ level, whose position is calculated from the polarization formula Eq. (7). The solid line in Fig. 2 represents this equation with the present values for the parameters, while the points show the experimental levels. The small displacement of the $7i$ point simply reflects the rounding error of energy levels to three decimal places. For the other points, the error bar represents the experimental uncertainty of 0.003 cm^{-1}. Clearly the fit is excellent.

For comparison, the four new energy levels of BB, namely $5g$, $6g$, $7g$, and $7h$ are about 0.02 cm^{-1} lower than mine. The discrepancy simply reflects the position of the $4f$ levels, which are 0.018 cm^{-1} lower in EI than in the present work. The difference in turn is due to the positions of the $3d$ and the $4d$ levels, which have HFS of the same order as the discrepancy (Table 2). Thus, the importance of fully accounting for the HFS in the present work is clearly demonstrated. In the same Table 3 of BB, the quantum defects of the g levels are seen to vary over 10%. In stark contrast, Fig. 2 shows that the quantum defects which are proportional to $\Delta_p/P(n,l)$ change by merely 0.1% for the same g levels. Here the discrepancy is due primarily to the different IP adopted with EI's value being 0.11 cm^{-1} below mine.

In Fig. 3 the same plot is displayed for the nf levels, where the last two values are taken from the $3d$–nf transitions of EI, with the present values of the $3d$ levels. Evidently
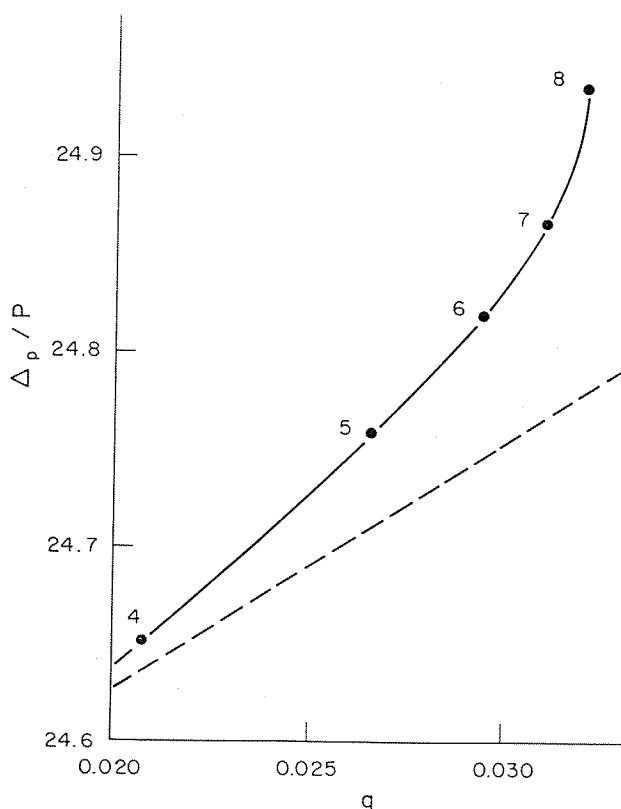

FIG. 3. Plot for polarization formula for the $l = 3$ levles. The dashed line is the the polarization formula of EI.

the data points do not fall on a straight line. For comparison, the polarization formula with EI's values for the parameters, $A = 24.301$ and $k = 0.646$ is shown as the dashed line. While our values for A differ only by 1.5%, our k values have opposite signs!

The discrepancy can be traced primarily to the difference in our values for the ionization potential. In effect, EI imposed a linear fit to the nf polarization plot by treating the IP as a free parameter. One sees that the data in Fig. 3 can be forced into roughly a straight line by a constant decrease of Δ_p, since $P(n,l)$ decreases with n. Indeed from the new measurements[15] for the $3d\,^2D-nf\,^2F$ series where n ranges from 11 to 55 at a lower accuracy of 0.05 cm^{-1}, a higher ionization potential was inferred. The value of 48 278.42 cm^{-1} lies about half way between EI's and the present value. Returning to the high-resolution data in Fig. 3, the upward curvature of the actual data is due to the $3s3p3d\,^2F$ state imbedded in the continuum which causes a downward repulsion of the higher member of the nf series. On the other hand, Fig. 2 shows that perturbations are absent for the higher l states as expected.

6. Conclusions

The present compilation of the energy levels of Al I is made from high-precision data measured in the last decade. I estimated the accuracy to be 0.003 cm^{-1}, which represents about an order of magnitude improvement over earlier compilations,[1,2] as the discrepancy is often in the 0.01 to 0.03 cm^{-1} range. The present work explicitly accounts for the hyperfine splittings which have recently been accurately measured.[3-6] Other data utilized come from the Fourier transform spectra of Brault and collaborators[7,8] which are accurate to the third decimal place. They are analyzed with proper accounting of the HFS in the low-l transitions.

The study of the high-l transitions allows for a new determination of the ionization potential. The new value is significantly higher than the old one, as was the case[10] for Mg I. It is now clear that the old method of evaluating the IP from extrapolating the nf series[1] is inherently inaccurate. Instead higher l data with the requisite precision is needed. In Al I, the fitting of high-l ($l \geqslant 4$) data to the polarization formula yields a negative value for k, as was found to be the case for every atom investigated (Mg[10], O[15], and He[16]). The implication is that the effect of nonadiabatic correction to the dipole polarizability always exceeds that of the quadrupole polarizability. Only in the case of helium can this be demonstrated theoretically.[17]

7. References

[1] K. B. S. Eriksson and H. G. S. Isberg, Arkiv Fysik **23**, 527 (1963).

[2] W. C. Martin and R. Zalubas, J. Phys. Chem. Ref. Data **8**, 817 (1979).

[3] Z. K. Jiang, H. Lundberg, and S. Svanberg, Phys. Lett. A **92**, 27 (1982).

[4] Ch. Belfrage, S. Horback, C. Levinson, I. Lindgren, H. Lundberg, and S. Svanberg, Z. Phys. A **316**, 15 (1984).

[5] G. Jonsson, S. Kroll, H. Lundberg, and S. Svanberg, Z. Phys. A **316**, 259 (1984).

[6] B. Falkenberg and P. Zimmermann, Z. Naturforsch. **34a**, 1249 (1979) and references therein.

[7] E. Biemont and J. W. Brault, Phys. Scr. **35**, 286 (1986).

[8] J. W. Brault and R. Noyes, Astrop. J. **269**, L61 (1983); E. S. Chang and R. Noyes, Astrop. J. **275**, L11 (1983).

[9] B. Edlen, Phys. Scr. **17**, 565 (1978).

[10] E. S. Chang, Phys. Scr. **35**, 792 (1987).

[11] L. Davis, B. T. Feld, C. W. Zabel, and J. R. Zacharias, Phys. Rev. **76**, 1076 (1949).

[12] Y. Y. Zhao, J. Carlsson, H. Lundberg, and G. G. Wahlstrom, Z. Phys. D **3**, 365 (1986).

[13] A. R. Edmunds, *Angular Momentum in Quantum Mechanics* (Princeton University, Princeton, N.J., 1957), p. 119 (with appropriate modification).

[14] H. A. Bethe and E. E. Salpeter, *Quantum Mechanics of One and Two Electron Atoms* (Academic, New York, 1957), p. 110.

[15] A. N. Zherikhin, V. I. Mishin, and V. N. Fedoseev, Opt. Spektrask **51**, 783 (1984).

[16] E. S. Chang, W. M. Barowy, and H. Sakai, Phys. Scr. **38**, 22 (1988); note in proof.

[17] E. S. Chang, Phys. Rev. **35**, 2777 (1987).

[18] R. J. Drachman, Phys. Rev. **26**, 1228 (1982).